GEOPHYSICS, VOL. 65, NO. 4 (JULY-AUGUST 2000); P. 1142–1153, 17 FIGS., 2 TABLES.

A comparison of the correlation structure in GPR images of deltaic and barrier-spit depositional environments

Paulette Tercier*, Rosemary Knight*, and Harry Jol‡

ABSTRACT

We have used geostatistical analysis of radar reflections to quantify the correlation structures found in 2-D ground-penetrating radar (GPR) images. We find that the experimental semivariogram, the product of the geostatistical analysis of the GPR data, is well-defined and can be modeled using standard geostatistical models to obtain an estimate of the range or correlation length, and the maximum correlation direction, in the 2-D GPR image. When we compare the results from geostatistical analysis of GPR data from selected deltaic and barrier-spit depositional environments we find different correlation structures in GPR images from different depositional environments. GPR images from braid deltas have near-horizontal correlation directions and correlation lengths on the order of a few meters. In contrast, the GPR image of a fan-foreset delta has a very long (>24 m) correlation length and a maximum correlation direction plunging 20°. In the GPR images from barrier spits, we find maximum correlation directions that are horizontal or plunging a few degrees. The correlation lengths range from 7 to 43 m, depending on the orientation of the GPR image relative to spit end growth, and on the specific radar facies that is analyzed.

INTRODUCTION

A common objective in many applied problems in the earth sciences is to generate an accurate model of the spatial variation in physical and chemical properties of the subsurface. This can involve the integration of different types of data, such as surface geophysics, borehole measurements, and direct sampling. In many cases, the data coverage is insufficient, and we need some way to "fill in" between data points. A common approach is to use geostatistical methods to account for the spatial variability that exists in natural, heterogeneous geological environments.

Geostatistics provides a mathematical framework which can be used to describe how some property or parameter varies spatially; these spatial statistics can then be used in the development of the subsurface model. Some information about spatial statistics can be obtained from borehole data or cores, but this usually only provides a good measure of variation in the vertical direction. To obtain a description of lateral variation, data can be collected from "analog" outcrops, selected as representative of the subsurface geology, but this is extremely time-consuming and usually limited to the two dimensions of the exposed outcrop. An alternate approach is the use of ground penetrating radar (GPR), a high-resolution geophysical technique which can be used to image the shallow subsurface in two or three dimensions. GPR images provide information about the sampled volume of the shallow subsurface and can also be used in the way data from analog outcrops are used, when the imaged near-surface modern and ancient systems are considered representative of, or analogous to, deeper sedimentary sections.

Several publications have described the use of 2-D and 3-D GPR images to obtain information about the lithologic variation and internal structure of sedimentary systems; some recent examples include Gawthorpe et al. (1993), Pratt and Miall (1993), Beres et al. (1995), Bristow et al. (1996), Jol et al. (1996), and McMechan et al. (1997). Our interest is in obtaining quantitative information about the spatial statistics of a region of the subsurface through geostatistical analysis of GPR data. The methodology we use is that developed and described in the paper by Rea and Knight (1998) where the sampled parameter in the geostatistical analysis is the amplitude of the reflections in the GPR data. Through our analysis, we obtain a model of the correlation structure of the GPR reflections. Our working hypothesis is that the correlation structure of the GPR image can be used to model the spatial variability in the physical and chemical properties of the subsurface.

In this study, we analyze GPR data from selected deltaic and barrier-spit depositional environments. It was shown in Rea and Knight (1998) that GPR images of glaciofluvial deposits have well-defined correlation structures that can be accurately described using standard geostatistical models. The

Manuscript received by the Editor October 16, 1998; revised manuscript received August 23, 1999.
*University of British Columbia, Dept. of Earth and Ocean Sciences, 2219 Main Hall, Vancouver, B.C. V6T 1Z4, Canada. E-mail: knight@geop.ubc.ca.
‡University of Wisconsin–Eau Claire, Dept. of Geography, 105 Garfield Avenue, Eau Claire, Wisconsin 54702-4004.

first objective of the present study is to determine whether geostatistics can be successfully applied to analyzing GPR data from these other environments. If geostatistics is found to provide a useful way of describing the GPR images, the second objective is to determine whether different depositional environments have different correlation structures when imaged with GPR.

DESCRIPTION OF SELECTED GPR SECTIONS

For this study, we have chosen a number of previously published radar data sets from different deltaic and barrier-spit depositional environments. Detailed descriptions of the acquisition, processing, and interpretation of the sections can be found in the referenced papers. The GPR sections from deltaic deposits include the Box Elder Creek fan-foreset delta (Smith and Jol, 1992a) and the American Fork River braid delta (Jol and Smith, 1992) in Utah, the Athabasca River braid delta in Alberta (Jol and Smith, 1992), and the William River wave-dominated delta in Saskatchewan (Jol, 1995). GPR sections from barrier-spit sites that were chosen for study include the Willapa Bay spit located in Washington (Jol et al., 1994) and the Sandy Point spit in Alberta (Smith and Jol, 1992b).

All radar data sets were collected using a pulseEKKO IV radar system with 100-MHz antennas. For all surveys, the antenna spacing was set to 1 m, whereas station spacing ranged from 0.5 to 1.0 m depending on the survey. Processing of the GPR data was conducted using the software available from Sensors and Software. GPR data were first processed to correct for signal saturation using a residual mean filter. Time zero corrections were made for shifts due to electronic drift. A single common-midpoint (CMP) survey was conducted at each site to determine a subsurface velocity which was used to convert the collected time sections to depth sections. A summary of the velocity used for each data set is given in Table 1. As a final step, the data were gained using an automatic gain function.

It is important to note that all GPR sections used in this study are 2-D sections. We are not conducting a full 3-D analysis of the correlation structure of the imaged sediments, but are sampling a specific plane through the sedimentary sequence and analyzing the structure captured in that slice through the subsurface. Each GPR section is oriented so as to provide an image of a specific location and orientation within the depositional environment under study.

METHOD FOR GEOSTATISTICAL ANALYSIS OF GPR DATA

An excellent introduction to geostatistics can be found in Isaaks and Srivastava (1989). In our work, we use the semivariogram, a plot which illustrates the way in which the difference between data values is related to the distance between the data values. The experimental semivariogram is described by the following equation (Journel and Huijbregts, 1978):

$$\hat{\gamma}(\mathbf{h}) = \frac{1}{2N}\sum_{i=1}^{N}[z(\mathbf{x_i}+\mathbf{h}) - z(\mathbf{x_i})]^2, \qquad (1)$$

where $\mathbf{h}$ is the lag, or separation vector, between two data points, $z(\mathbf{x_i}+\mathbf{h})$ and $z(\mathbf{x_i})$, and N is the number of data pairs used in each summation. The direction selected for $\mathbf{h}$, for construction of the semivariogram, is commonly the direction of maximum correlation. In our geostatistical analysis of the GPR data, we use the amplitude values recorded in the radar traces to construct the experimental semivariogram. The details of the method are given in Rea and Knight (1998).

An underlying assumption in semivariogram analysis is that the data under analysis conform to a concept referred to as "stationarity." Stationarity implies that any subset of the data will have the same statistical description as any other subset. In radar data sets, two separate stationarity issues must first be addressed: attenuation of the radar signal with depth, and the occurrence of more than one geological facies in the radar profile. The first issue has to do with the radar signal itself. The signal in all the traces in a GPR profile will attenuate with depth. This will produce a systematic trend in the data and violate stationarity. To overcome this problem (the attenuation of the signal with depth), we use an automatic gain control (AGC) with a short window length to transform all amplitudes of reflections to approximately the same value. The high-amplitude signals caused by the air and ground arrivals are removed by cropping the data. The second stationarity issue has to do with the facies changes found in sedimentary sequences due to varying depositional processes. Data sets which contain more than one facies are divided so that semivariogram analysis can be completed on each facies separately. As we have no way of directly sampling the subsurface material, the division is based on the concept of radar facies, where a radar facies is defined as a unit which has a characteristic radar signature (Jol and Smith, 1991; Beres and Haeni, 1991; Rea and Knight, 1995; van Overmeeran, 1996).

We use a modified version (Jian et al., 1996) of the program gamv2m in the software GSLIB (Deutsch and Journel, 1992) to calculate the experimental semivariogram. Among the important input parameters within gamv2m are angular tolerance and bandwidth. Angular tolerance is the half-angle tolerance on the lag vector, $\mathbf{h}$; bandwidth is the vertical distance measured perpendicular to the lag vector. These two parameters help define the area to be searched when looking for pairs to be used in the semivariogram calculation. Setting the angular tolerance or bandwidth too high will result in an increase in the number of pairs found as the lag increases. Although this will smooth out the experimental variogram, it may also result in a shorter correlation length. For all sections, we set the bandwidth and angular tolerance to a minimum number while still enabling points to be found at all lags. As suggested by Journel and Huijbregts (1978), we limited the maximum lag considered in the experimental semivariogram to half the domain size or observation length in the GPR profile.

Semivariogram models are used to provide an analytic description of the experimental semivariogram. We considered a number of the more commonly used models: the exponential, spherical, pentaspherical, Gaussian, cubic, and power models, and the nugget effect. Equations for all these models can be

Table 1. Subsurface velocity for GPR sections.

GPR section	Velocity (m/ns)
American Fork River	0.13
Athabasca River	0.13
William River	0.07
Box Elder Creek	0.14
Willapa Bay	0.07
Sandy Point	0.08

found in Journel and Huijbregts (1978) and McBratney and Webster (1986). While these models are generally used simply as an empirical means of describing the data, a discussion of the theoretical basis for some of the models is given by McBratney and Webster (1986). The exponential model can be shown to describe the semivariogram which will result from a variety of processes such as first-order Markov processes (Agterberg, 1970; McBratney and Webster, 1986), and is the model that is often assumed by researchers in stochastic hydrology (Woodbury and Sudicky, 1991). The semivariograms from 11 of the 16 GPR sections in our study were best described using the exponential model, which is given by

$$\gamma(h) = C\left(1 - e^{-\frac{3h}{a}}\right), \qquad \text{if } 0 < h$$
$$\gamma(0) = 0, \tag{2}$$

where C is referred to as the sill, and a, referred to as the range, is the distance at which the data values are no longer correlated and is equivalent to the correlation length of the data set.

Many semivariograms exhibit a discontinuity at the origin. This is most commonly attributed to structure in the data set that is on a scale smaller than the sampling interval. The discontinuity can be modeled using the nugget effect, which can be included in the equations for the semivariogram models. The equation describing the exponential model with a nugget effect is

$$\gamma(h) = C_0 + C\left(1 - e^{-\frac{3h}{a}}\right), \qquad \text{if } 0 < h$$
$$\gamma(0) = 0, \tag{3}$$

where C_0 is referred to as the nugget.

Three GPR sections were modeled using the spherical or pentaspherical models with the nugget effect. These are described by the following equations (Journel and Huijbregts, 1978; McBratney and Webster, 1986). The spherical model with a nugget effect is given by

$$\gamma(h) = C_0 + C\left[\frac{3h}{2a} - \frac{1}{2}\left(\frac{h}{a}\right)^3\right], \qquad \text{if } 0 < h \le a,$$
$$\gamma(h) = C_0 + C, \qquad \text{if } h > a,$$
$$\gamma(0) = 0. \tag{4}$$

The pentaspherical model with a nugget effect is given by

$$\gamma(h) = C_0 + C\left[\frac{15h}{8a} - \frac{5}{4}\left(\frac{h}{a}\right)^3 + \frac{3}{8}\left(\frac{h}{a}\right)^5\right], \qquad \text{if } 0 < h \le a,$$
$$\gamma(h) = C_0 + C, \qquad \text{if } h > a,$$
$$\gamma(0) = 0. \tag{5}$$

The weighted least squares procedure, as outlined in Jian et al. (1996), was used to find the model parameters. This procedure minimizes R, the weighted square difference between the experimental data and the semivariogram model, and is defined by

$$R = [\hat{\gamma} - \gamma]^{\mathrm{T}}\mathbf{V}^{-1}[\hat{\gamma} - \gamma], \tag{6}$$

where $\mathbf{V}^{-1}$ is the diagonal matrix of weights; the variance matrix was used for $\mathbf{V}$. The decision as to which model best fits the data was made by considering two parameters: the sum of the squares of the weighted differences, R, and the Akaike information criterion, AIC. The AIC is given by

$$\mathrm{AIC} = n \ln\left(\frac{R}{n}\right) + 2p, \tag{7}$$

where n is the number of points in the experimental semivariogram and p is the number of parameters in the model. When comparing models for any one data set, the model with the smallest AIC is the best model.

For each of the 2-D GPR images, we first determine the direction of maximum correlation and define our lag vector as oriented in this direction. The modeled semivariogram in this direction thus reveals the maximum correlation length of the radar reflections in the 2-D GPR section. An interesting extension of this work would be to obtain full 3-D radar images and define the complete 3-D correlation structure. What we have done in this study allows us to assess the structure in specific planes in different depositional environments.

RESULTS AND DISCUSSION

We found, in all cases, that geostatistical analysis of the GPR sections produced semivariograms of outstanding quality—both in terms of the form of the variogram and in terms of the agreement with the selected model. We discuss each of the GPR sections in detail below. Table 2 presents a summary of the parameters used in the geostatistical analysis and the modeling results. Table 2 gives for each GPR section the direction of the lag vector (which is equivalent to the maximum correlation direction for the section) with angular tolerance, and the bandwidth; the best fit model with the model parameters (range and nugget); and the values of R and AIC used in determining the best model. In the three cases where the exponential model was not the best model, we also include (for comparison purposes) the results of fitting the data with an exponential model.

Deltaic examples

Figure 1 shows GPR data collected over the American Fork River braid delta. The GPR section is oriented perpendicular to the direction of last delta growth. The reflections seen in this data set have been qualitatively described as distinct, continuous to semicontinuous wavy reflections (Jol and Smith, 1992). These short reflections have been interpreted to represent an environment of channel scour and deposition (Jol et al., 1996) which exists as the braided river changes course across the delta. The boundaries observed in the GPR profiles probably represent bounding discontinuities which may include contacts between beds and sedimentary structures, channel scours, and the base and top of stratigraphic units.

The rectangle drawn on Figure 1 outlines the area used in the geostatistical analysis. The maximum correlation direction was found to be along a line plunging approximately 0.5° north. Figure 2 shows the experimental semivariogram calculated in that direction. The result in Figure 2 is a classic example of a semivariogram. Unlike many geostatistical studies where the lack of data points makes it very difficult to accurately define the semivariogram, the large number of data points in

the GPR data gives us this "textbook" example of a semivariogram. Each data point in the semivariogram is the result of averaging between 10 000 and 19 500 data pairs. These data are modeled using an exponential model with a range of 3 m, and show excellent agreement with that model.

Another example of a braid river delta is shown in Figure 3. These data, taken from the publication by Jol and Smith (1992), were collected over the Athabasca River delta located at the Embarras Airfield in northeastern Alberta. The GPR section in this case is oriented parallel to the direction of last delta growth. Once again the GPR image is dominated by short, discontinuous reflections indicative of a sedimentary environment where there are recurring episodes of scour and deposition. This long profile provides us with the opportunity to assess how variable the correlation structure of GPR data can be in a braid river delta. For the geostatistical analysis, the 600-m profile was divided into four sections: A, B, C and D, each 150 m in length, as shown in Figure 3. The direction of maximum correlation varied among the areas from a line plunging 1° west-northwest to a line plunging 1° east-southeast. Figure 4 shows the semivariograms corresponding to the areas indicated by the rectangles in Figure 3. All areas were modeled using an exponential model with ranges equal to 6 m for section A, 4 m for section B, 5 m for section C, and 4 m for section D. We find that the 2-D GPR sections from both the American Fork and Athabasca braid river deltas are characterized by short, subhorizontal reflections with correlation lengths of 3 to 6 m.

Table 2. Semivariogram analysis: parameters and results.

Environment and Location			Area analyzed	Orientation of lag vector (°)	Bandwidth (m)	Model*	Range (m)	Nugget	*R*	AIC
Deltas	Braid	American Fork R.		0.5 ± 2.98 N	0.026	exp.	3	0.02	0.007	–163
		Athabasca River	A	1 ± 1.49 W-NW	0.026	exp.	6	0.22	0.003	–133
			B	1 ± 1.49 E-SE	0.026	exp.	4	0.14	0.004	–126
			C	1 ± 1.49 E-SE	0.026	exp.	5	0.14	0.002	–137
			D	0	—	exp.	4	0.01	0.002	–139
	Wave	William River	A	1 ± 0.80 E	0.014	exp.	7	0.21	0.003	–121
			B	2 ± 0.80 E	0.014	pent. exp.	14 18	0 0	0.01 0.04	–182 –149
	Fan-Foreset	Box Elder Creek		20 ± 2.83 NW	0.026	—	> 24	—	—	—
Spits	Marine	Willapa Bay		1.5 ± 0.80 W	0.014	exp.	24	0.03	0.003	–314
				0	—	—	> 30	—	—	—
	Lacustrine	Sandy Point	A'	1 ± 0.92 SE	0.016	pent. exp.	16 15	0.10 0.04	0.03 0.07	–229 –205
			A"	0	—	sph. exp.	7 7	0.10 0	0.03 0.03	–150 –146
			B'	2 ± 0.92 SE	0.016	exp.	7	0	0.01	–238
			B"	3 ± 0.92 SW	0.016	exp.	10	0.04	0.01	–112
			C'	0	—	exp.	43	0.16	0.01	–411
			C"	2 ± 0.92 SW	0.016	exp.	9	0.08	0.03	–170

*exp. = exponential, pent. = pentaspherical, sph. = spherical, *R* = sum of squares of weighted difference, AIC = Akaike information criterion.

The radar profile shown in Figure 5 is an example of GPR data collected over a wave-dominated delta. This profile was collected along strike over the modern William River delta located in northern Saskatchewan and clearly shows two radar facies (Jol, 1995). For geostatistical characterization, the section has been split into these two separate radar facies. The upper radar facies (A) is characterized by wavy, discontinuous reflections. These have been interpreted as upper shoreface and beach foreshore deposits, where the sediments deposited are constantly reworked by waves and longshore currents. The maximum correlation direction for the reflections in this radar facies on the 2-D GPR section was found to be along a line plunging 1° east. The semivariogram calculated in this direction is shown in Figure 6a. The experimental semivariogram is best modeled using an exponential model with a range of 7 m. The lower radar facies (B) is dominated by gently inclined reflections which have been interpreted as representing the middle lower shoreface, which was farther from the shore than the sediments imaged in area A of this GPR section. Semivariogram analysis of this facies revealed a maximum correlation direction along a line plunging at 2° east. The experimental semivariogram in Figure 6b was best fit using a pentaspherical model with a range equal to 14 m. For comparison purposes, the data also were fit using an exponential model; this model results in a range equal to 18 m and values of R and AIC that are not significantly different from those obtained for the pentaspherical model.

Figure 7 shows an example of GPR data collected over a fan-foreset delta (taken from Smith and Jol, 1992a). These data were collected in the Brigham City Sand and Gravel Company pit floor and show the late Pleistocene Box Elder Creek delta. Fan-foreset deltas are dominated by steeply inclined strata, referred to as foreset beds, which are preserved as the delta progrades into deep water. Typically, one finds horizontally bedded sediments (referred to as topset and bottomset beds, respectively) lying both above and below the package of foreset beds. In the GPR data presented from this location, however, only the foreset beds are imaged. The topset beds have been excavated, and the radar signal is attenuated before it reaches the bottomset beds. A number of GPR profiles were collected over the package of foreset beds, oriented perpendicular to the strike of the frontal slope. The GPR section shown in Figure 7 is the one which shows the steepest apparent dip of the foreset beds.

Data within the rectangle in Figure 7 were used in the geostatistical analysis. The direction of maximum correlation within this 2-D image was found to be along a line plunging 20° to the northwest. Figure 8 shows the experimental semivariogram obtained with a lag vector oriented in this direction. Given the length and depth of the GPR section, the maximum lag that could be used in constructing the semivariogram was 24 m. [As stated in the description of our procedure, we follow the suggestion of Journel and Huijbregts (1978) that the maximum lag not exceed half the observation length in the data set.] As the experimental semivariogram in Figure 8 shows, even at a lag of 24 m there is not any apparent flattening to suggest that

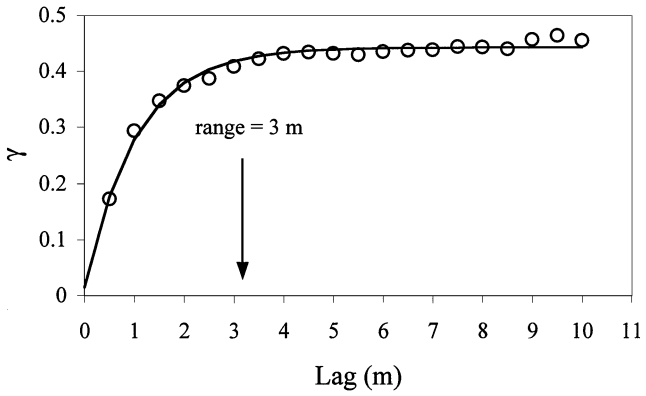

FIG. 2. Semivariogram analysis of the GPR image shown in Figure 1. Circles = experimental data; solid line = the model of the semivariogram. These data are modeled using an exponential model with a range of 3 m.

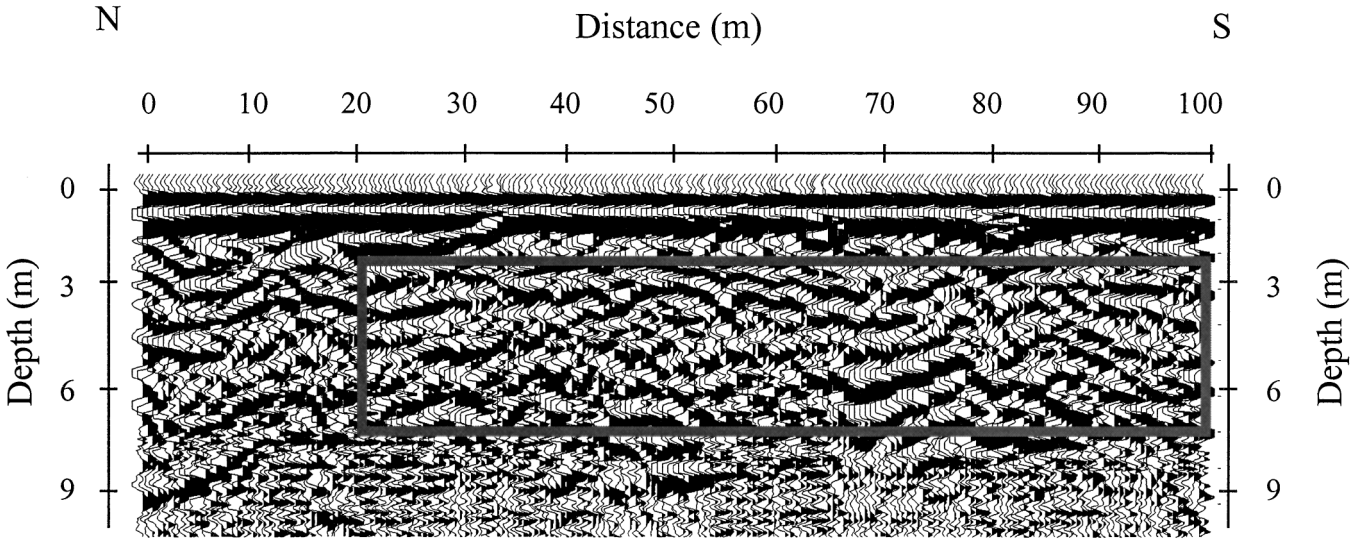

FIG. 1. GPR profile collected over the American Fork River braid delta (modified from Jol and Smith, 1992). The data found within the rectangle are used in the geostatistical analysis.

we have reached the range. We can only conclude from this example that the range in this GPR section is greater than 24 m.

It is important to note that in order to get an accurate determination of the maximum correlation direction and length in this GPR data set, where the reflections are plunging relatively steeply, the data should first be migrated. While migration of the data had no effect on the determined correlation structure in the other examples (which have reflections that are close to horizontal in orientation), migration of the data in this example changes the maximum correlation direction from a plunge angle of 20° to 21°. Migration would also decrease the correlation length of the GPR image. For example, if the determined range in this data set was actually 24 m in the unmigrated data, this would be decreased to 21 m in the migrated data set.

Geostatistical analysis of the 2-D GPR sections from the three types of deltas show differences in both the maximum correlation direction and length. The GPR image of the foreset delta is dominated by steeply inclined continuous reflections with a maximum correlation direction of 20° and a correlation length >24 m. In contrast, the GPR images of the braid deltas are characterized by shorter subhorizontal reflections with maximum correlation directions between 0.5° and 1° and ranges between 3 m and 6 m. The GPR image of the wave-dominated delta is also characterized by subhorizontal reflections with maximum correlation directions between 1° and 2° but with ranges for the two radar facies of 7 m and 18 m.

Barrier-spit examples

Figures 9 and 10 show GPR profiles collected over a marine coastal barrier spit located in Willapa Bay, Washington (Jol et al., 1994). The spit end is growing in a direction which parallels the shoreline, while progradation of the spit is occurring in a direction perpendicular to the shoreline. The GPR profile in Figure 9 was collected perpendicular to the direction of spit-end growth. The gently inclined reflections in this profile have been interpreted as beach foreshore strata and represent the shingle-like accretionary layers of sediment that forms as the spit progrades seaward. Figure 11 shows the results from the semivariogram analysis of this section. The GPR data from this environment provide an outstanding example of an experimental semivariogram that shows close to perfect agreement with the model. The direction of maximum correlation is along a line plunging 1.5° west. An exponential model with a range of 24 m is used to fit the data.

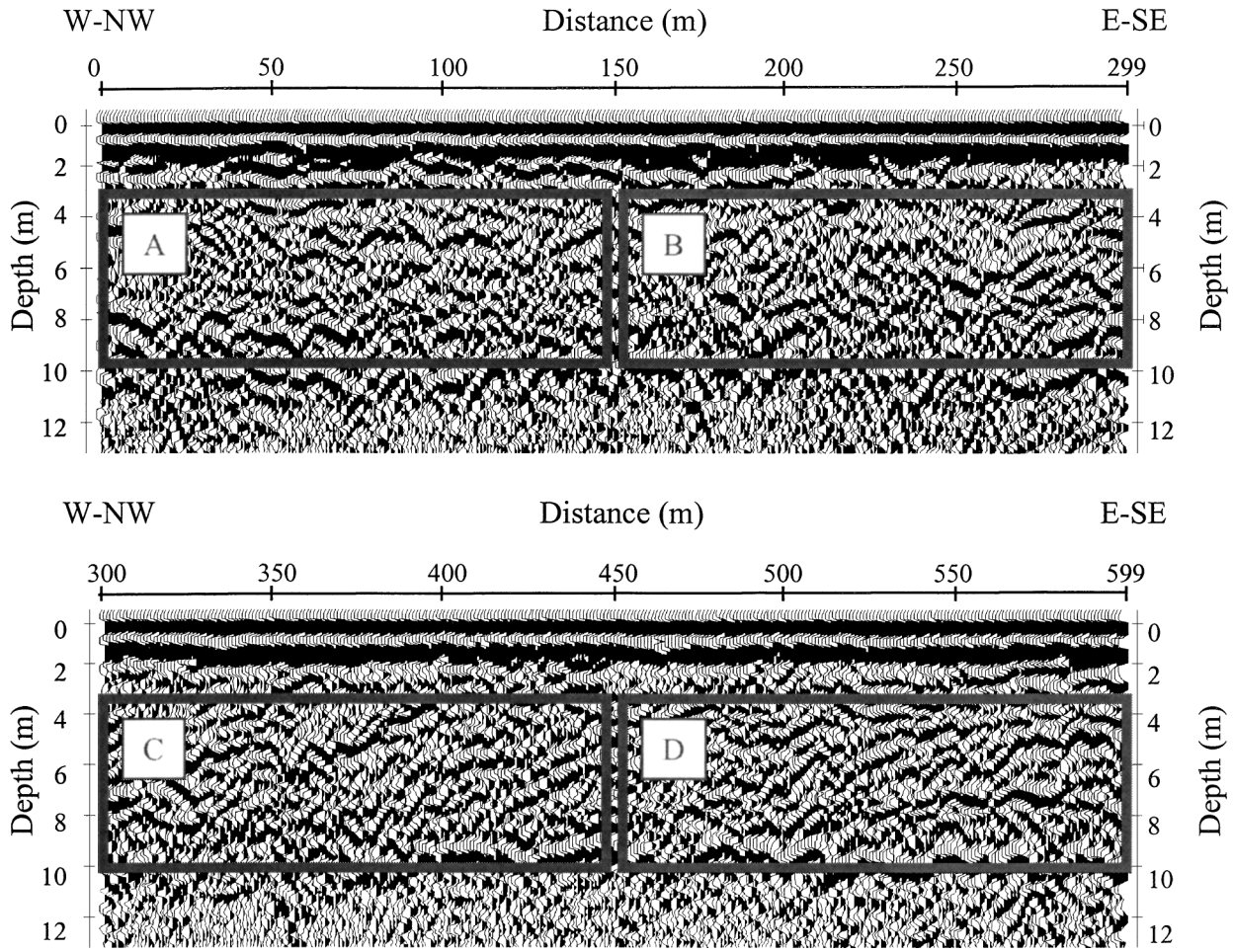

FIG. 3. GPR profile collected over the Athabasca River braid delta in northeastern Alberta. The lower profile is a continuation of the profile above. The data found within rectangles A, B, C, and D were used in the geostatistical analysis.

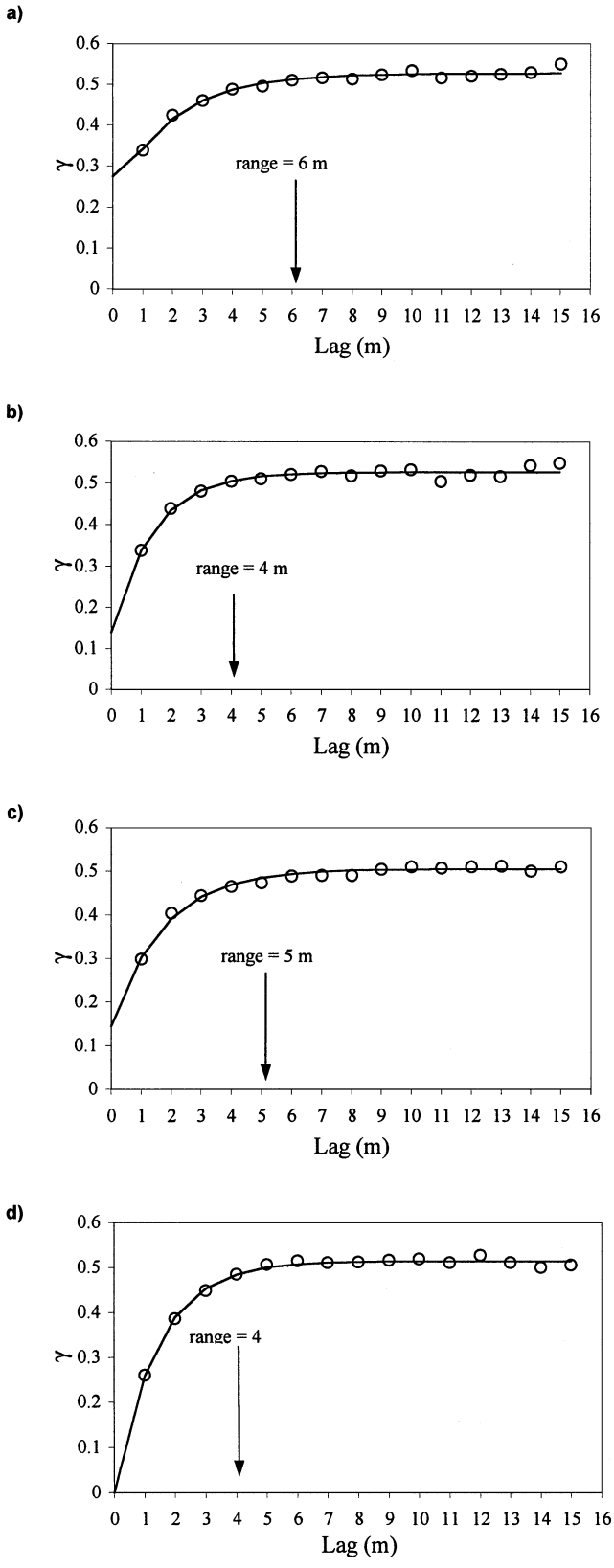

FIG. 4. Semivariogram analysis of the GPR image shown in Figure 3. Circles = data points; solid line = the model of the semivariogram. In all cases, the data were modeled using an exponential model. (a) The reflections in area A have a range equal to 6 m. (b) The reflections in area B have a range equal to 4 m. (c) The reflections in area C have a range equal to 5 m. (d) The reflections in area D have a range equal to 4 m.

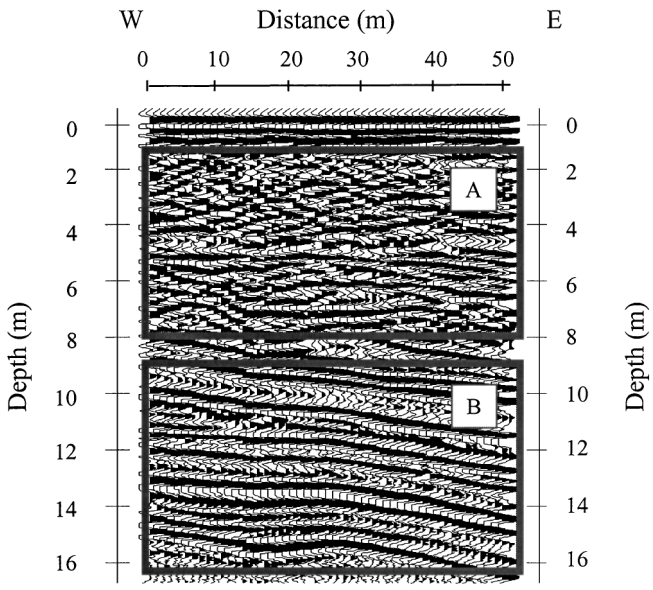

FIG. 5. GPR data collected over the William River wave-dominated delta in northern Saskatchewan (modified from Jol, 1995). Two radar facies have been identified: "A" represents reflections in the beach foreshore/upper shoreface, "B" represents reflections in the middle lower shoreface. The data found within the two rectangles were used in the geostatistical analysis.

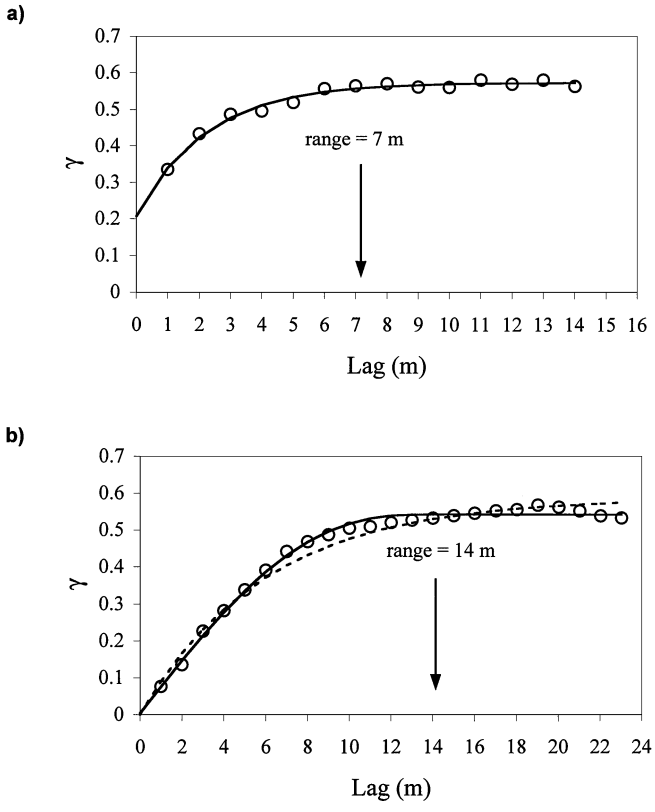

FIG. 6. Semivariogram analysis of the GPR image shown in Figure 5. Circles = data points; solid line = the best fit model of the semivariogram. (a) The data from area A are modeled using an exponential model with a range of 7 m. (b) The data from area B are best modeled using a pentaspherical model with a range of 14 m. The data are also fit with an exponential model (broken line) with a range equal to 18 m.

The GPR section in Figure 10 was collected along a line parallel to the direction of spit-end growth. In this profile, the shingle-like layers are represented by long continuous horizontal reflections across most of the section. Figure 12 contains the semivariogram obtained with a lag vector aligned in the direction of maximum correlation, in this case horizontal. This experimental semivariogram has not been modeled as there is no apparent flattening of the semivariogram. From these data, we can only determine that the range is greater than 30 m.

The collection of the GPR data parallel and perpendicular to the direction of spit-end growth has allowed us to characterize the correlation structure of the GPR image in these two directions. For the Willapa Bay spit, we find that the correlation length of reflections in the direction parallel to spit-end growth is greater than that in the direction perpendicular to spit-end growth.

Figures 13 and 14 show GPR data from the active lacustrine Sandy Point spit located near Fort Chipewyan in northeastern Alberta (Smith and Jol, 1992b). These profiles have been collected along lines parallel (Figure 13) and perpendicular (Figure 14) to the direction of spit-end growth. This active spit is prograding southeastward into Lake Athabasca. Longshore currents from the northeast transport sediment to the distal end of the spit. Smith and Jol (1992b) identified four radar facies based on the reflection patterns in the GPR profiles. The lowermost radar facies occurs at depths >12.5 m. The highly attenuated signals in this facies are interpreted to represent lacustrine mud. Because the signal has been attenuated, no geostatistical analysis is presented for this facies.

The first radar facies is the upper 0–3 m of the radar profiles shown in Figures 13 and 14. This radar facies contains horizontal to slightly inclined reflections which are interpreted to represent beach foreshore and upper shoreface deposits. Regions of the GPR sections that correspond to this radar facies are labeled A′ on the section parallel to spit-end growth and A″ on the section perpendicular to spit-end growth. Semivariogram analysis of A′ revealed a maximum correlation direction along a line plunging 1° southeast. Figure 15a shows the experimental semivariogram calculated in this direction. These data are best fit using a pentaspherical model with a range equal to 16 m. For comparison purposes, the data also are modeled using an exponential model with the range equal to 15 m. Figure 15b shows the semivariogram for region A″ calculated in the horizontal direction, which is the direction of maximum correlation. These data are best modeled using a spherical model with a range of 7 m. The data can also be modeled very well with an exponential model with a range of 7 m.

Geostatistical analysis of the two perpendicular sections from both the marine Willapa Bay spit and the lacustrine Sandy Point spit found that the direction of maximum correlation in all four of the 2-D GPR images of the beach foreshore strata was very shallow, ranging from 0° to 1.5°. For both spits, the correlation lengths were longer in the direction parallel to spit-end growth than in the direction perpendicular to spit-end growth.

The second radar facies, shown in Figures 13 and 14 in the regions labeled B′ and B″, consists of inclined reflections which are interpreted to represent the middle to lower shoreface. The GPR image in region B′ was found to have a maximum correlation direction plunging 2° southeast. The experimental

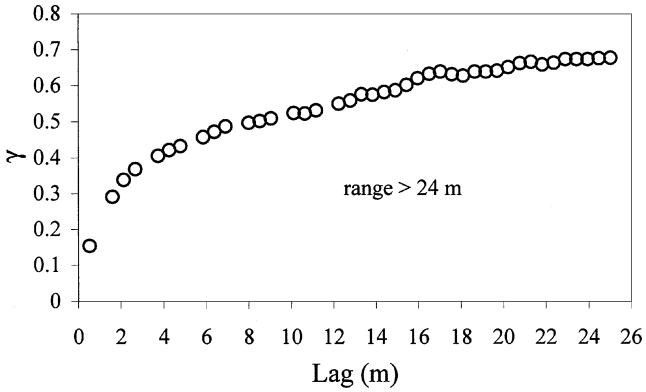

FIG. 8. Experimental semivariogram of the GPR data collected over the Box Elder Creek delta foreset beds shown in Figure 7. These data have not been modeled as there is no clear flattening of the sill. The value of 24 m is taken as a lower bound on the range.

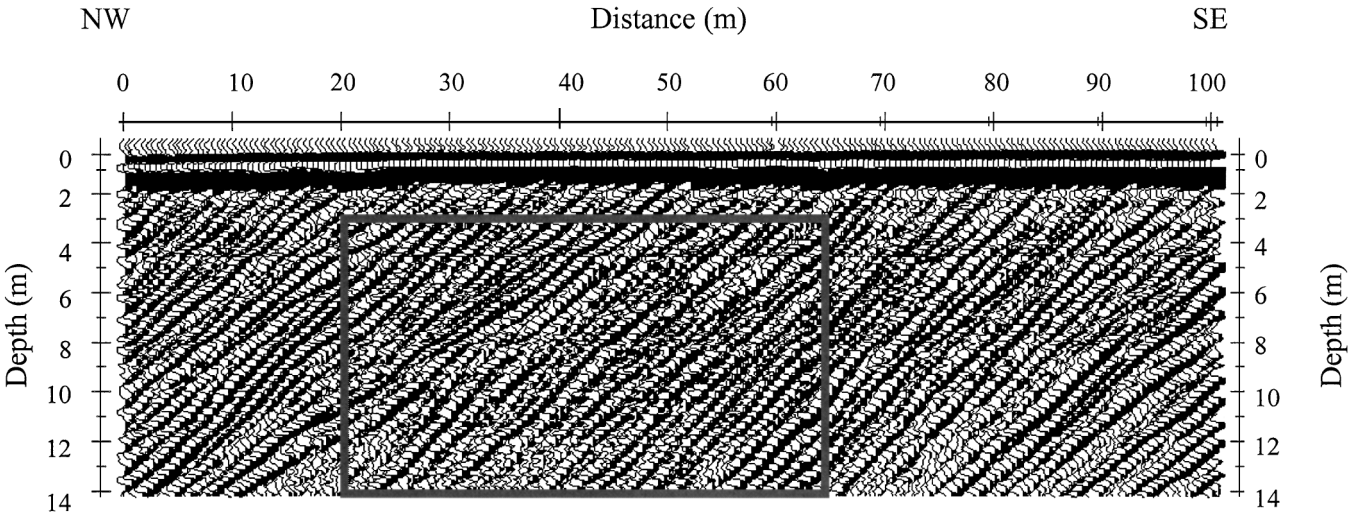

FIG. 7. GPR profile collected over the Box Elder Creek fan-foreset delta in Utah (modified from Smith and Jol, 1992a). Data within the rectangle were used in the geostatistical analysis.

semivariogram for region B′ is shown in Figure 16a. These data are best fit with an exponential model with a range corresponding to 7 m. The maximum correlation direction for the reflections in the region labeled B″ was found to be along a line plunging 3° southwest. The semivariogram for B″ is shown in Figure 16b. These data are modeled using an exponential model with a range of 10 m. The correlation lengths of the reflections within the middle lower shoreface are very similar for the data both parallel and perpendicular to the direction of spit-end growth: 7 m for B′ and 10 m for B″.

The final radar facies is shown in Figures 13 and 14 as C′ and C″. These continuous, horizontal reflections of this radar facies have been interpreted to represent the lake bed. The experimental semivariogram shown in Figure 17a has been calculated along the horizontal; this corresponds to the direction of maximum correlation for C′. The semivariogram is best modeled using an exponential model with a range of 43 m. Shown

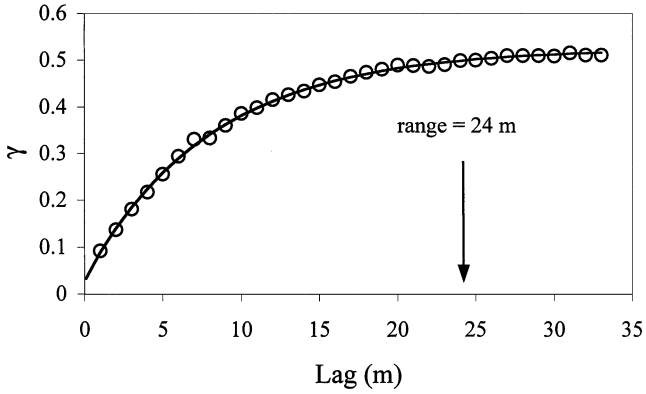

FIG. 11. Semivariogram analysis of the GPR image shown in Figure 9. Circles = data points; solid line = the model of the semivariogram. The data are modeled using an exponential model with a range of 24 m.

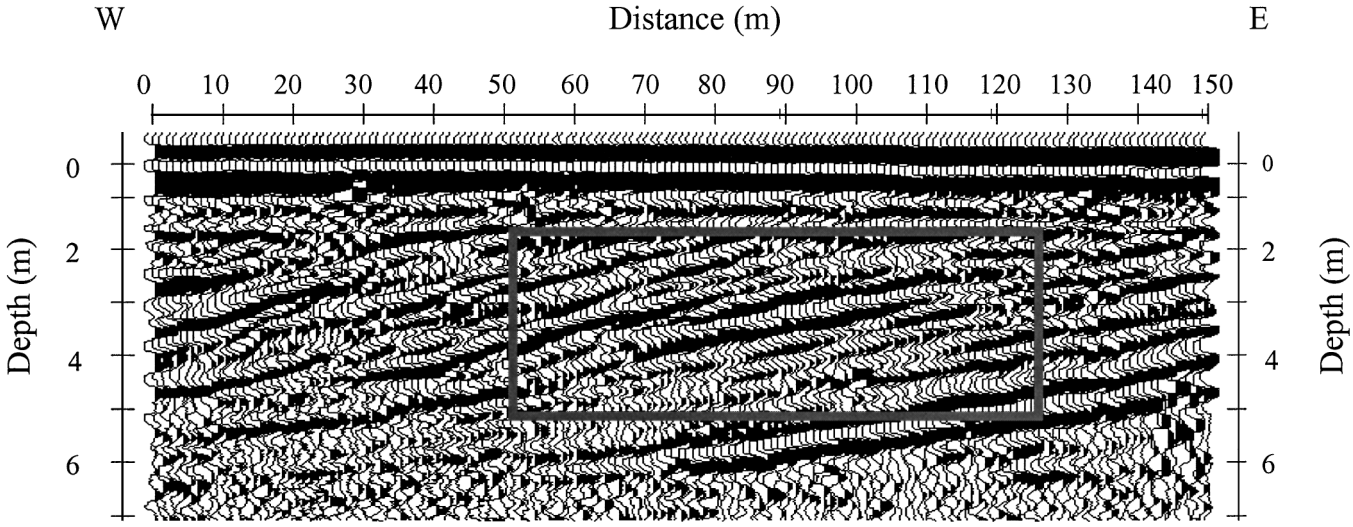

FIG. 9. GPR profile collected over the Willapa Bay coastal barrier spit along a line perpendicular to the direction of spit-end growth (modified from Jol et al., 1994). The rectangle indicates data used in the geostatistical analysis.

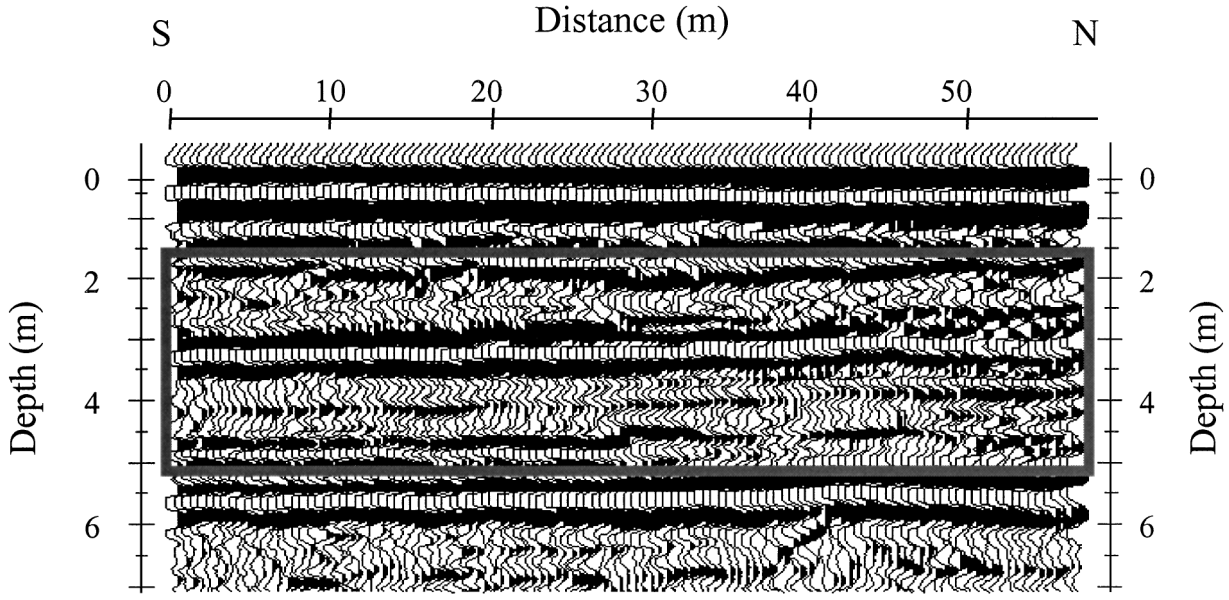

FIG. 10. GPR profile collected over the Willapa Bay coastal barrier spit along a line parallel to the direction of spit-end growth (modified from Jol et al., 1994). The rectangle indicates data used in the geostatistical analysis.

in Figure 17b is the semivariogram calculated using the data in region C″ collected perpendicular to the direction of spit-end growth. This semivariogram was calculated along the direction of maximum correlation, a line plunging 2° southwest. These data are best modeled using an exponential model with a range of 9 m. The long subhorizontal reflections with correlation lengths ranging from 9 to 43 m are interpreted to represent the build-up of sediments along the lakebed. The longer range of 43 m corresponds to the direction of longshore drift.

CONCLUSIONS

We have found that the spatial variability in GPR images can be well described using standard geostatistical models, and that geostatistical analysis of GPR data gives us an effective way of quantifying the correlation structure of the GPR image. Such geostatistical information can be useful in developing models of the subsurface, either for the region imaged with GPR or

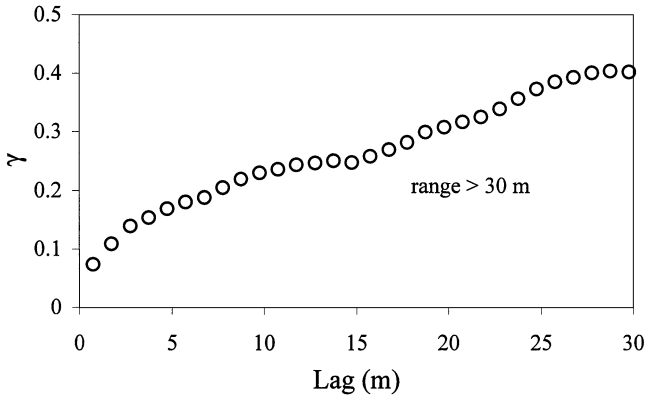

FIG. 12. Semivariogram analysis of the GPR image shown in Figure 10. Circle = data points. These data have not been modeled as there is no clear flattening of the sill. A lower bound on the range can be set at 30 m.

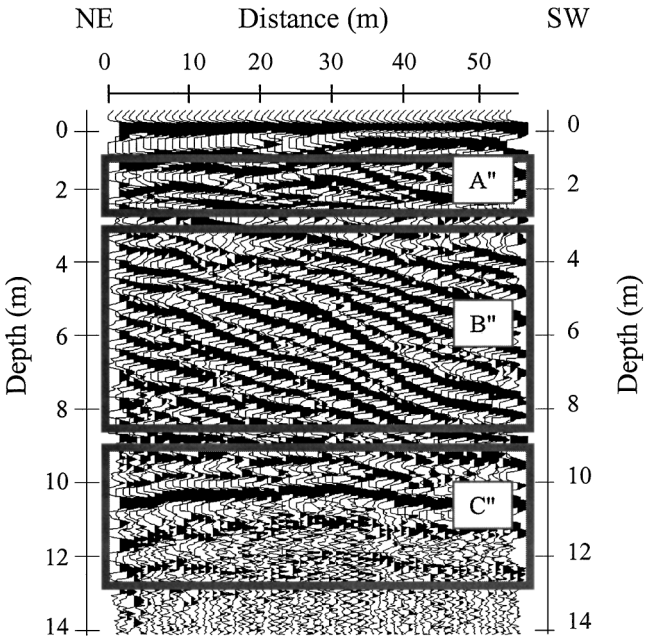

FIG. 14. GPR profile collected over the active Sandy Point spit along a line perpendicular to the direction of spit-end growth (modified from Smith and Jol, 1992b). The three rectangles indicate the data used in the geostatistical analysis. Area A″ represents beach foreshore/upper shoreface, area B″ represents middle lower shoreface, and area C″ represents the lake bed.

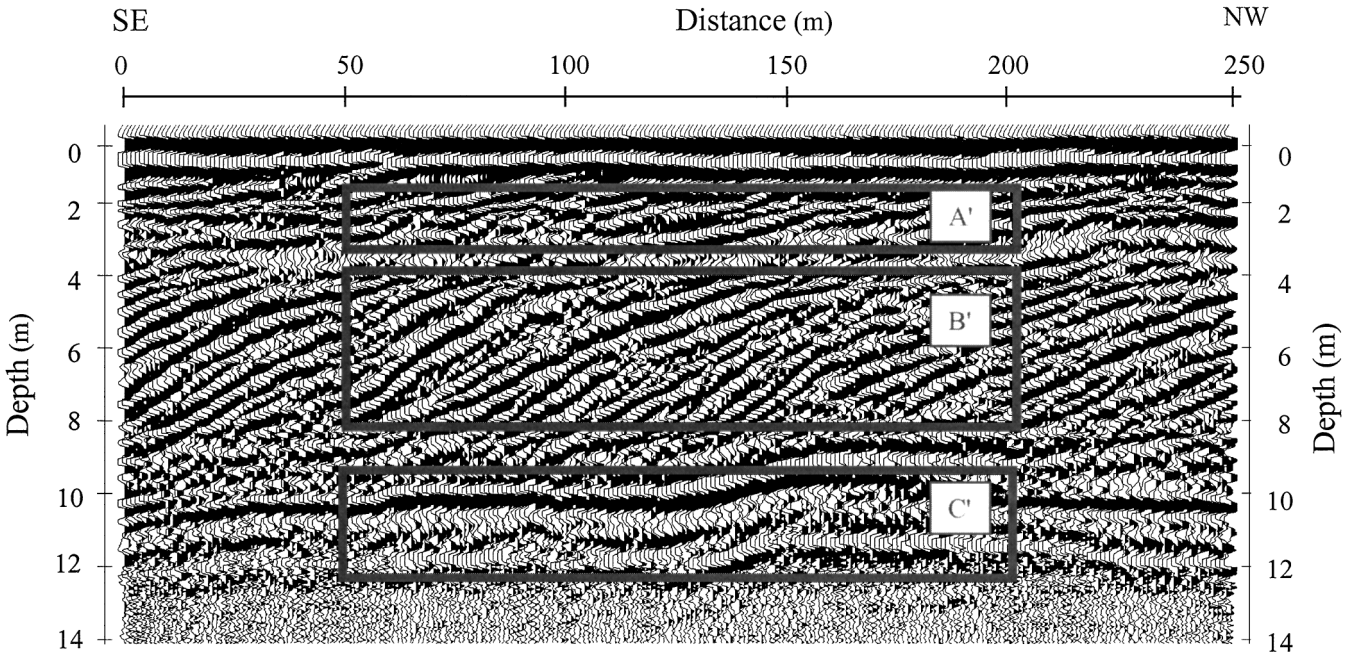

FIG. 13. GPR profile collected over the active Sandy Point spit along a line parallel to the direction of spit-end growth (modified from Smith and Jol, 1992b). The three rectangles indicate the data used in the geostatistical analysis. Area A′ represents beach foreshore/upper shoreface, area B′ represents middle lower shoreface, and area C′ represents the lake bed.

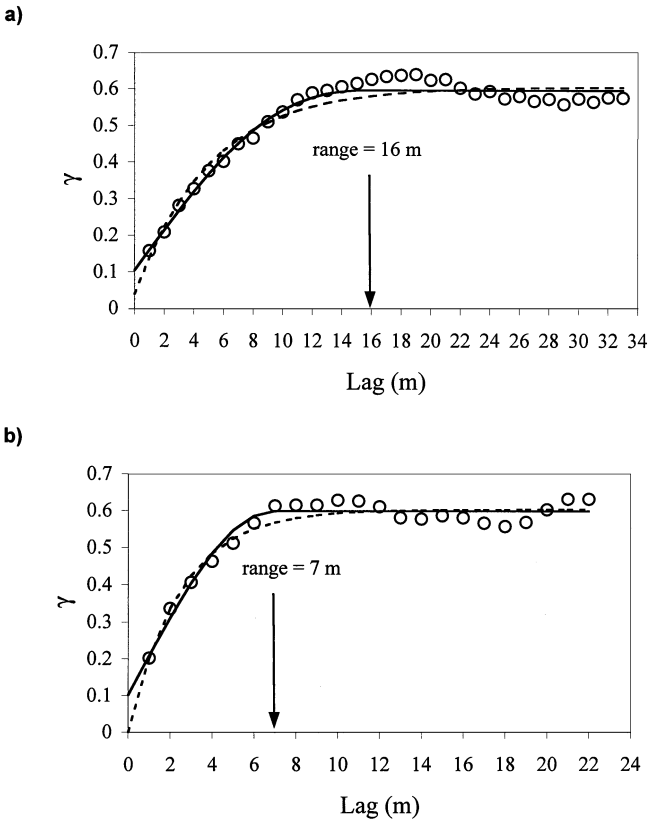

FIG. 15. Semivariogram analysis of areas A′ and A″ shown in Figures 13 and 14. Circles = data points; solid line = the best fit model of the semivariogram. (a) The data from area A′ are best modeled using a pentaspherical model with a range of 16 m. These data can also be modeled very well using an exponential model (broken line) with a range equal to 15 m. (b) The data from area A″ are best modeled using a spherical model with a range of 7 m. These data can also be modeled very well using an exponential model (broken line) with a range equal to 7 m.

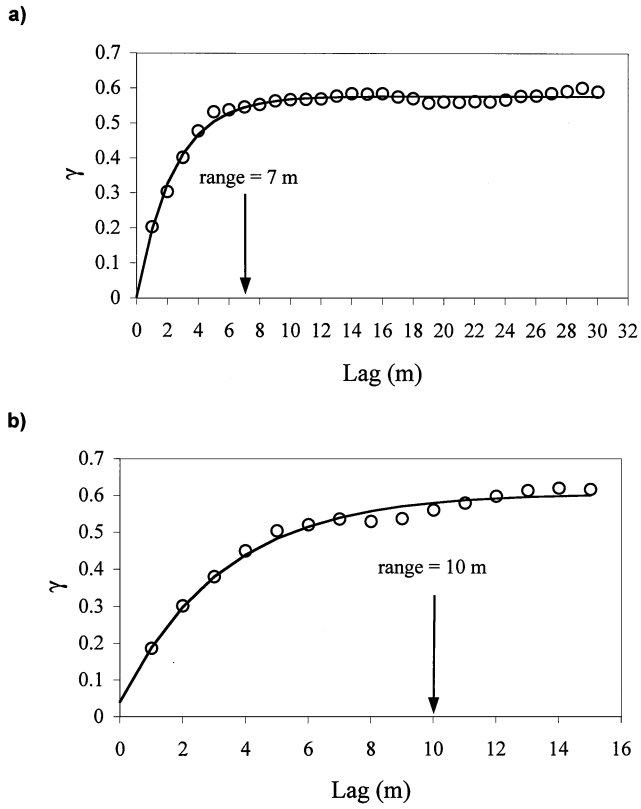

FIG. 16. Semivariogram analysis of areas B′ and B″ shown in Figures 13 and 14. Circles = data points; solid line = the model of the semivariogram. (a) The data from area B′ are modeled using an exponential model with a range of 7 m. (b) The data from are area B″ are modeled using an exponential model with a range of 10 m.

for other regions (such as deep hydrocarbon reservoirs) that can be considered analogous to the imaged section.

The geostatistical analysis of the GPR sections clearly reveals the presence of different correlation structures in GPR images of different depositional environments. This study has been a start in describing and comparing the correlation structure seen in GPR images from such different environments. We suggest that the correlation structures of GPR images are closely related to the processes that formed the imaged geologic section. In order to develop a fundamental theoretical framework to explain such observations, we will ultimately need to unravel the complex relationships between sedimentary processes, spatial variation in sedimentological parameters, and the corresponding variation in dielectric properties that is imaged in the GPR data.

ACKNOWLEDGMENTS

Funding for this research came from Amoco Canada, Conoco, Esso Resources, Pan Canadian, Petrel-Robertson, Petro-Canada, Natural Sciences and Engineering Council of Canada, Norcen Energy Resources, Western Geophysical, the University of Wisconsin-Eau Claire, and Sensors and Software. This work has also been supported at the University of British Columbia by the U.S. Air Force Office of Scientific Research, Air Force Material Command, USAF, under grant number F49620-95-I-0166. The views and conclusions contained herein are those of the authors and should not be interpreted as necessarily representing the official policies or endorsements, either expressed or implied, of the Air Force Office of Scientific Research or the U.S. government. Derald Smith and Rick Meyers (University of Calgary) are acknowledged for their field support, and Christian Scullard (University of British Columbia) for the development of the program used in the variogram modeling.

REFERENCES

Agterberg, F. P., 1970, Autocorrelation functions in geology, *in* Merriam, D. F., Ed., Geostatistics: Plenium, 113–141.

Beres, M., and Haeni, F. P., 1991, Application of ground-penetrating-radar methods in hydrogeologic studies: Ground Water, **29**, 375–386.

Beres, M., Green, A., Huggenberger, P., and Horstmeyer, H., 1995, Mapping the architecture of glaciofluvial sediments with three-dimensional georadar: Geology, **23**, 1087–1090.

Bristow, C., Pugh, J., and Goodall, T., 1996, Internal structure of aeolian dunes in Abu Dhabi determined using ground-penetrating radar: Sedimentology, **43**, 995–1003.

Deutsch, C. V., and Journel, A. G., 1992, GSLIB geostatistical software library and user's guide: Oxford Univ. Press.

Gawthorpe, R. L., Collier, R. E. L., Alexander, J., Bridge, J. S., and Leeder, M. R., 1993, Ground penetrating radar: Application to

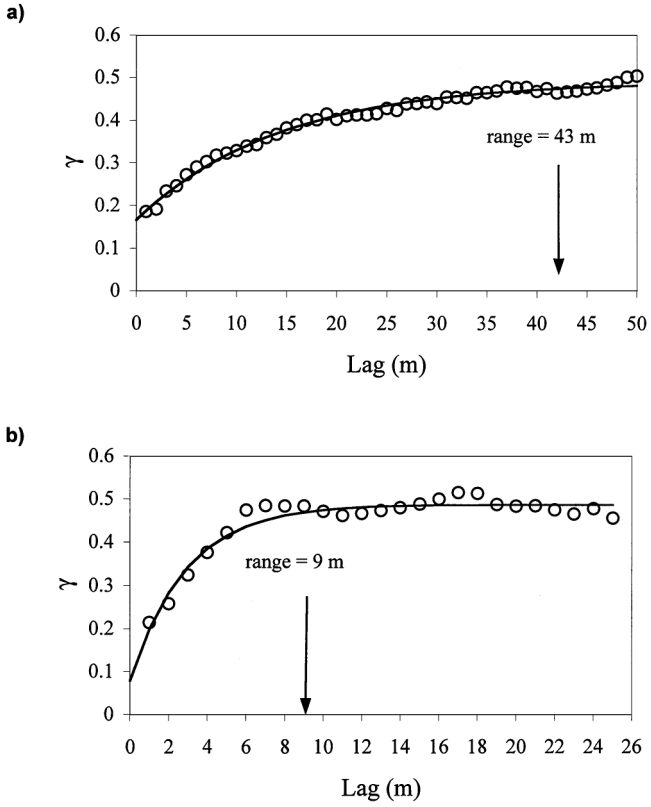

FIG. 17. Semivariogram analysis of areas C′ and C″ shown in Figures 13 and 14. Circles = data points; solid line = the model of the semivariogram. (a) The data from area C′ are modeled using an exponential model with a range of 43 m. (b) The data from area C″ are modeled using an exponential model with a range of 9 m.

sandbody geometry and heterogeneity studies, *in* North, C. P. and Prosser, D. J., Eds., Characterization on fluvial and aeolian reservoirs: Geol. Soc. Spec. Pub. **73**, 421–432.
Isaaks, E. H., and Srivastava, R. M., 1989, An introduction to applied geostatistics: Oxford Univ. Press.
Jian, X., Olea, R. A., and Yu, Y., 1996, Semivariogram modeling by weighted least squares: Comput. and Geosci., **22**, 387–397.
Jol, H. M., 1995, Ground penetrating radar antennae frequencies and transmitter powers compared for penetration depth, resolution and reflection continuity: Geophys. Prosp., **43**, 693–709.
Jol, H. M., Meyers, P. A., Lawton, D. and Smith, D., 1994, A detailed GPR investigation of a coastal barrier spit, Long Beach, Washington, U. S. A.: SAGEEP, Ann. Mtg., Env. Eng. Geophys. Soc., 107–127.
Jol, H. M., and Smith, D. G., 1991, Ground penetrating radar of northern lacustrine deltas: Can. J. Earth Sci., **28**, 1939–1947.
——— 1992, Geometry and structure of deltas in large lakes: A ground penetrating radar overview: Geol. Surv. Finland, Spec. Pap. **16**, 159–168.
Jol, H. M., Smith, D. G., Meyers, R. A., and Lawton, D. C., 1996, Ground penetrating radar: High resolution stratigraphic analysis of coastal and fluvial environments, *in* Pacht, J. A., Sheriff, R. E., and Perkins, B. F., Eds., Stratigraphic analysis utilizing advanced geophysical, wireline and borehole technology for petroleum exploration and production: Presented at GCSSEPM Foundation 17th Ann. Res. Conf., 153–163.
Journel, A. G., and Huijbregts, Ch. J., 1978, Mining geostatistics: Academic Press Inc.
McBratney, A. B., and Webster, R., 1986, Choosing functions for semivariograms of soil properties and fitting them to sampling estimates: J. Soil Science, **37**, 617–639.
McMechan, G. A., Gaynor, G. C., and Szerbiak, R. B., 1997, Use of ground-penetrating radar for 3-D sedimentological characterization of clastic reservoir analogs: Geophysics, **62**, 786–796.
Pratt, B. R., and Miall, A. D., 1993, Anatomy of a bioclastic grainstone megashoal (Middle Silurian, southern Ontario) revealed by ground penetrating radar: Geology, **21**, 223–226.
Rea, J. M., and Knight, R. J., 1995, The use of ground penetrating radar for aquifer characterization: An example from southwestern British Columbia: Symposium on the application of geophysics to engineering and environmental problems: Env. and Eng. Geophys. Soc., 279–288.
Rea, J., and Knight, R. J., 1998, Geostatistical analysis of ground-penetrating radar data: A means of describing spatial variation in the subsurface: Water Resources Res., **34**, 329–339.
Smith, D. G., and Jol, H. M., 1992a, Ground-penetrating radar investigation of a Lake Bonneville delta, Provo level, Brigham City, Utah: Geology, **20**, 1083–1086.
——— 1992b, GPR results used to infer depositional processes of coastal spits in large lakes: Geol. Surv. Finland, Spec. Pap. **16**, 169–177.
van Overmeeren, R. A., 1996, Radar facies of unconsolidated sediments in the Netherlands: A radar stratigraphic interpretation method for hydrogeology: 6th Internat. Conf. Ground Penetrating Radar, Expanded Abstracts, 167–172.
Woodbury, A. D., and Sudicky, E. A., 1991, The geostatistical characteristics of the Borden aquifer: Water Resources Res., **27**, 533–546.